Journal of Power Sources 268 (2014) 106–112

Contents lists available at ScienceDirect

Journal of Power Sources

journal homepage: www.elsevier.com/locate/jpowsour

Short communication

# Towards understanding the rate capability of layered transition metal oxides $LiNi_yMn_yCo_{1-2y}O_2$

Zheng Li [a, 1, 2], Chunmei Ban [b, 2], Natasha A. Chernova [a], Zhuangchun Wu [b], Shailesh Upreti [a], Anne Dillon [b, 3], M. Stanley Whittingham [a, *]

[a] Institute for Materials Research, State University of New York at Binghamton, Binghamton, NY 13902, USA
[b] National Renewable Energy Lab, 1617 Cole Boulevard, Golden, CO 80401, USA

## HIGHLIGHTS

- The Li diffusivities of $Li_xNi_yMn_yCo_{1-2y}O_2$ increase with increasing Co amount.
- $Li_xNi_{0.33}Mn_{0.33}Co_{0.33}O_2$ shows higher electronic conductivity than $Li_xNi_{0.5}Mn_{0.5}O_2$.
- The rate performance were understood in terms of diffusivity and conductivity.

## ARTICLE INFO

*Article history:*
Received 1 March 2014
Received in revised form
29 May 2014
Accepted 29 May 2014
Available online 6 June 2014

*Keywords:*
Lithium-ion battery
Rate capability
Lithium diffusion
Electronic conductivity

## ABSTRACT

This work attempts to understand the rate capability of layered transition metal oxides $LiNi_yMn_yCo_{1-2y}O_2$ ($0.33 \leq y \leq 0.5$). The rate capability of $LiNi_yMn_yCo_{1-2y}O_2$ increase with increasing Co in the compounds and with increasing amount of carbon additives in the electrodes. The lithium diffusion coefficients and electronic conductivities of $Li_xNi_yMn_yCo_{1-2y}O_2$ are investigated and compared. The 333 compound has higher diffusivity and electronic conductivity and thus better rate performance than 550. Chemical diffusion coefficients for both delithiation and lithiation of $Li_xNi_yMn_yCo_{1-2y}O_2$ investigated by GITT and PITT experiments are calculated to be around $10^{-10}$ $cm^2$ $s^{-1}$, lower than that of $Li_xCoO_2$. The electronic conductivity of $Li_xNi_yMn_yCo_{1-2y}O_2$ is inferior compared to $Li_xCoO_2$ at same temperature and delithiation stage. However, the $Li_xNi_yMn_yCo_{1-2y}O_2$ are able to deliver 55%–80% of theoretical capacity at 5 C with good electronic wiring in the composite electrode that make them very promising candidates for electric propulsion in terms of rate capability.



## 1. Introduction

The landmark cathode material $TiS_2$ for the first generation of rechargeable lithium-ion battery shows excellent high-rate performance even from today's point of view. In contrast to most current composite electrodes with conductive carbon additives, better rate performance was obtained in the carbon-free $TiS_2$ electrode [1,2]. This is largely attributed to the intrinsically high diffusivity ($10^{-8}$ $cm^2$ $s^{-1}$) [3] and metal-like electronic conductivity of $TiS_2$ ($5 \times 10^2$ S $cm^{-1}$ at around room temperature) [4]. The lack of high power-capability is one of the limiting factors for large-scale application of lithium ion batteries for electric propulsion or grid ancillary service like frequency regulations [5–8]. Therefore, the rate performance becomes one of the essential material selection criteria for lithium ion battery electrode materials. Enhanced rate capability may be achieved through improved lithium diffusivity [9] or improved intrinsic electronic conductivity [10,11] of the electrode materials. In a recent publication [12], Ban et al. have successfully improved the rate performance and cycle life of $LiNi_{0.4}Mn_{0.4}Co_{0.2}O_2$ to a surprising level via using Single-Wall Carbon Nanotubes (SWCNTs) as electronic wiring medium, which again stresses the important role of the electronic conductivity in the composite electrode [13,14].

Mixed transition metal oxides $LiNi_yMn_yCo_{1-2y}O_2$ ($0.33 \leq y \leq 0.5$, abbreviated as NMC) have been studied as possible alternatives to $LiCoO_2$ in terms of cost, toxicity and thermal stability. They also show better rate performance, thermal stability and cycle life than high capacity Li-rich oxides, i.e., $Li_{1+z}M_{1-z}O_2$ (M is transition metal)

* Corresponding author. Tel./fax: +1 607 777 4623.
*E-mail address:* stanwhit@binghamton.edu (M.S. Whittingham).
[1] Present address: Department of Materials Science and Engineering, Massachusetts Institute of Technology, Cambridge, MA 02139, USA.
[2] These authors contributed equally to this work.
[3] Deceased.

http://dx.doi.org/10.1016/j.jpowsour.2014.05.142
0378-7753/

[15]. The comparison of capacity, rate capability and cycle life for NMC has been investigated in previous studies [16–21]. Here we report a comparative study of the rate capability of $LiNi_yMn_yCo_{1-2y}O_2$ for $0.33 \le y \le 0.5$, where $y = 0.5$ is called 550, $y = 0.45$, 992, $y = 0.4$, 442 and $y = 0.33$, 333. This study determined the lithium diffusivity for both delithiation and lithiation process and the electronic conductivity as a function of lithium content.

## 2. Experiment

The $LiNi_yMn_yCo_{1-2y}O_2$ ($0.33 \le y \le 0.5$) was synthesized by the co-precipitation method followed by solid-state reaction at 800 °C as described earlier [16–18]. Samples for electronic conductivity measurements were prepared by pressing the 450 °C decomposed precursors into dense disk-shape pellets (10 mm diameter, 1 mm thickness) and sintering at 1100 °C (for 550) and 1000 °C (for 333) to ensure strength and density for the conductivity test. In order to delithiate the pellet, gold was sputtered on one side which served as a current collector to assemble a Swagelok™ cell, using lithium foil as anode. The cells were galvanostatically charged at 50 μA $cm^{-2}$ to the desired lithium content and relaxed for at least 3 days at zero current to gain homogeneity before being disassembled in the glove box.

Electrochemical properties were tested in 2325-type coin cells using Biologic VMP or VMP2 multichannel potentiostats. The cathode paste was made by mixing 80 wt% active material with 10 wt% carbon black and 10 wt% PVDF (poly(vinylidene fluoride)) in NMP (1-methyl-2-pyrrolidinone), unless specified otherwise. The loading of active material was around 6 mg $cm^{-2}$. To determine the impact of the carbon content, cathode pastes were also made with 30 wt% carbon black and 10 wt% PVDF with similar loadings of active material. The homogeneous paste was cast on aluminum foil then dried at 90 °C overnight in a vacuum oven. The electrolyte used was 1 M $LiPF_6$ (lithium hexafluorophosphate) in a 1:1 volume ratio mixture of DMC (dimethyl carbonate) and EC (ethylene carbonate) from Novolyte, USA. The coin cells were assembled in a helium-filled glove box. The cells were charged at 0.1 C to 4.3 V, then held at 4.3 V for 6 h before being discharged at different current rates.

The lithium chemical diffusion coefficient of $LiNi_yMn_yCo_{1-2y}O_2$ ($0.33 \le y \le 0.5$) was measured using the well-established Galvanostatic Intermittent Titration Technique (GITT) method on coin cells [22–25]. The cells were charged or discharged at 100 μA $cm^{-2}$ for 1 h then relaxed for 5 h following each pulse. The details of the calculation will be discussed later in this paper. The Potentiostatic Intermittent Titration Technique (PITT) was also used to investigate the lithium transport kinetics [26–28]. In the PITT measurements,

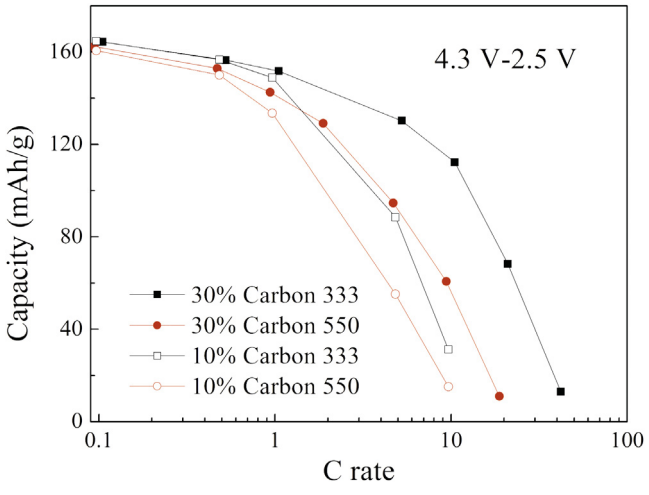


**Fig. 1.** The Ragone plot of 333 and 550 using different amount of carbon black, 10 wt% and 30 wt%. The C rate is equivalent to 1 mA $cm^{-2}$. All electrodes herein have a loading of active material around 6 mg $cm^{-2}$.

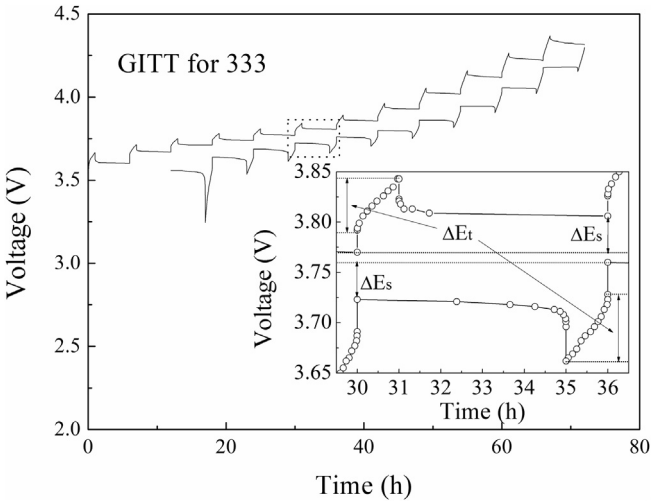


**Fig. 2.** The GITT experiment on 333 for both delithiation and lithiation process.

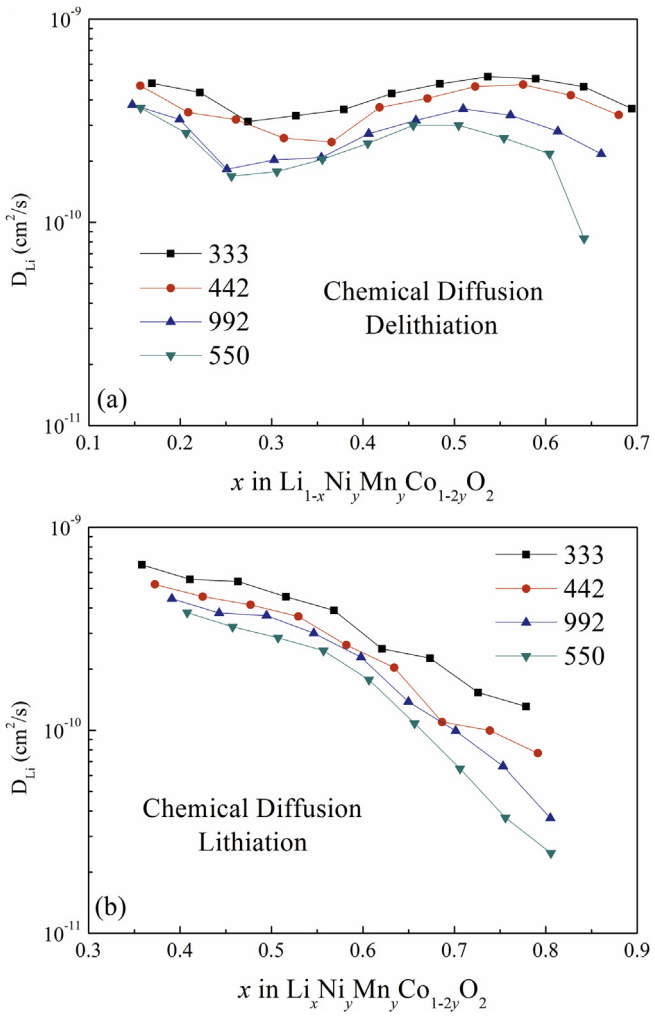


**Fig. 3.** The chemical diffusion coefficient $D_{GITT}$ of (a) delithiation and (b) lithiation for $Li_xNi_yMn_yCo_{1-2y}O_2$.

the cell voltage was raised in 20 mV increments up to 4.4 V and then lowered in 20 mV increments. Each voltage step was terminated when either the current decayed to a C/100 rate or after holding at constant voltage for more than 5 h.

The temperature-dependent electronic conductivity of the pristine and delithiated pellets was measured using a Quantum Design Physical Property Measurement System (PPMS). The temperature ranged from room temperature down to the temperature at which the resistance exceeded the measurable limit of the PPMS. For 550, the data were collected only from 300 K to 330 K due to the low conductivity. The as-obtained disk-shape samples were polished, cut into bar-shape (6–8 mm long with around 0.6–0.8 $mm^2$ cross-sectional area), and mounted on the specialized pucks of the PPMS. Two silver wires were affixed to the two smallest end faces using silver paste. The experiments were performed in a pure helium atmosphere.

The X-Ray Diffraction (XRD) patterns were obtained using a Scintag XDS2000 $\theta$–$\theta$ diffractometer equipped with a Cu-$K_\alpha$ radiation and a Ge(Li) solid state detector. The Rietveld refinement was done by using GSAS/EXPGUI package [29,30]. The morphology of the samples was examined by Scanning Electron Microscopy (EVO 50 variable pressure SEM, Zeiss).

## 3. Results and discussion

All the synthesized materials at 800 °C were shown to be single phase by x-ray diffraction with the following lattice parameters: 550, $a = 2.892$ Å, $c = 14.30$ Å; 992, $a = 2.882$ Å, $c = 14.29$ Å; 442, $a = 2.874$ Å, $c = 14.27$ Å; 333, $a = 2.863$ Å, $c = 14.25$ Å. For 550 synthesized at 1100 °C, $a = 2.888$ Å, $c = 14.30$ Å; 333 synthesized at 1000 °C, $a = 2.857$ Å, $c = 14.23$ Å. These are consistent with our previously published data [17], and the data by Dahn [31] and Ohzuku [32,33].

### 3.1. Electrochemical behavior

Unlike $TiS_2$, for electrochemical tests of $LiNi_yMn_yCo_{1-2y}O_2$, it is necessary to enhance the electronic conductivity of cathode composite electrodes, because the intrinsic conductivity of most cathode materials is much too low to allow them to be used alone. Typically carbon black is added to the active material together with a binder to hold the composite together. Fig. 1 shows the Ragone plots for discharge of the 333 and 550 compositions for carbon contents of 10 and 30 wt%. For both compositions the rate capability increases as the carbon content increases, suggesting that the electronic conductivity may be limiting. Even though the 550 composition has smaller average particle size of 50 nm, compared to the 100 nm of the 333 composition, it has lower capacity at the rates exceeding C/10.

### 3.2. Lithium diffusion

Both GITT and PITT techniques were used to determine the chemical diffusion coefficient, in order to understand the relationship between the observed rate capability and lithium diffusion rate. Even though chemical diffusion coefficients of the $Li_xNi_yMn_yCo_{1-2y}O_2$ compounds during charge (delithiation) have been reported [23–25], there is not much research on chemical diffusion coefficient during discharge (lithiation). Moreover, this is the first attempt to quantitatively compare the lithium diffusion kinetics of $Li_xNi_yMn_yCo_{1-2y}O_2$ as a function of increasing $y$. The well-studied $Li_xCoO_2$ is a two-phase reaction in the range of $0.75 \leq x \leq 0.93$ as lithium is extracted, then becomes one-phase diffusion-only reaction for $0.5 \leq x \leq 0.75$ [27,28]. The symmetrical charge/discharge voltage profile of $Li_xCoO_2$ between 3.0 V and 4.1 V shows less than 5 mV zero current voltage gap [14] and very small first cycle irreversible capacity. The diffusion coefficients for charge and

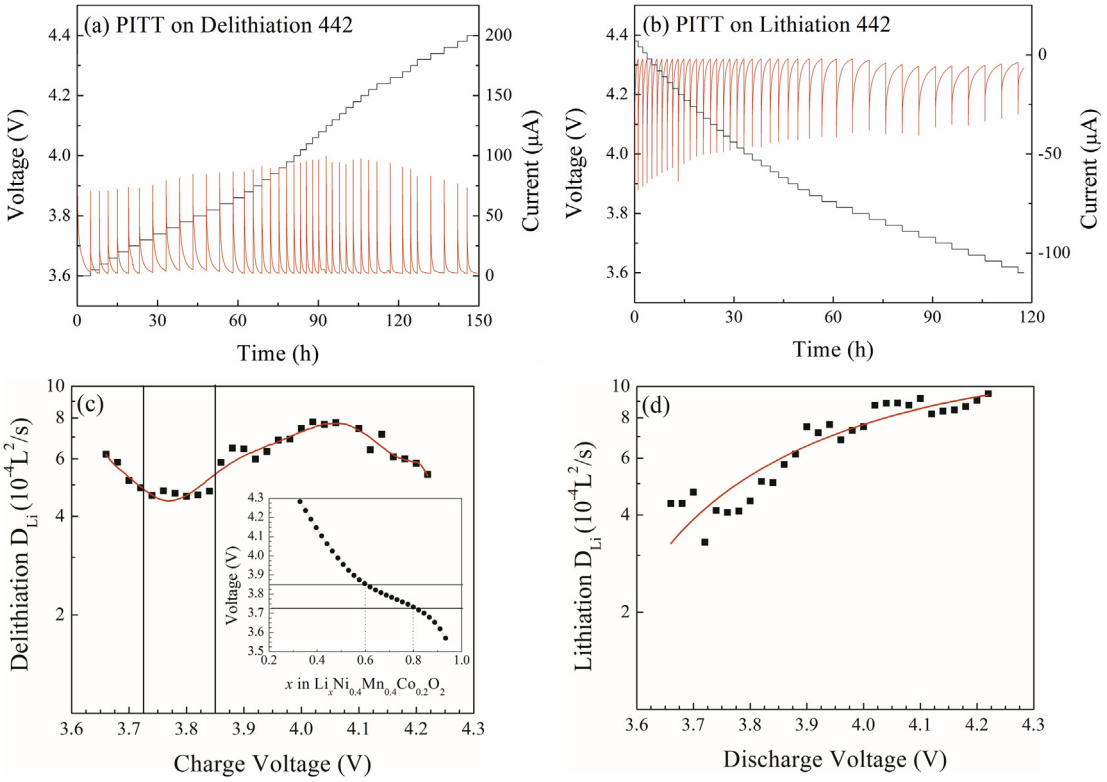


**Fig. 4.** The voltage steps $V(t)$ and corresponding current decay $I(t)$ under each constant voltage for 442 upon (a) delithiation and (b) lithiation. $D_{PITT}$ with respect to $L^2$ for 442 were calculated upon (c) delithiation and (d) lithiation.

discharge by PITT method are very close [27,28]. In contrast, $Li_xNi_yMn_yCo_{1-2y}O_2$ is a single phase reaction observed in both the continuous OCV profile [3,17] and the PITT current decay mode in the range $0.3 \leq x \leq 1$. Any phase transition, such as to the one block structure of $CoO_2$, only happens at high voltage, i.e. for $x \leq 0.3$ [25,34] and then only for the higher cobalt contents, such as 333, where there are no interlayer Ni pinning ions. Additionally, NMC electrodes show a significant first-cycle irreversible capacity. Therefore, different variation trends of chemical diffusion coefficients will be expected during charging and discharging $Li_xNi_yMn_yCo_{1-2y}O_2$ electrodes.

For the one-phase reaction, GITT measurement is very effective to determine the chemical diffusion coefficients. Fig. 2 shows the typical GITT curve of 333 for both charging and discharging. By applying Fick's second law to the diffusion system, the chemical diffusion coefficient in experimentally measurable form (Eq. (1)) can be obtained from the derived surface concentration with certain simplifying assumptions [25]:

$$D_{GITT} = \frac{4}{\pi\tau}\left(\frac{m_B V_m}{M_B S}\right)^2 \left(\frac{\Delta E_s}{\Delta E_\tau}\right)^2, \tau \ll L^2/D_{GITT} \quad (1)$$

where $\tau$ is the current pulse duration, $m_B$ is the mass of the active material, $V_m$ and $M_B$ are the crystallographic molar volume and the molecular weight of the compound, $S$ is the geometric area of interface between electrode and electrolyte, $L$ is the diffusion length, $\Delta E_\tau$ and $\Delta E_s$ are the transient voltage change during current pulse and the steady voltage change shown in the inset graph of Fig. 2. The units for $\tau$, $m_B$, $V_m$, $M_B$, $S$, $\Delta E_\tau$ and $\Delta E_s$ are s, g, $cm^3\ mol^{-1}$, $g\ mol^{-1}$, $cm^2$, V and V, respectively. In these studies we used for the value of S, the geometric area of the cell, 1.2 $cm^2$; the other extreme is to use the powder surface area as measured for example by the BET method. The true value is somewhere in between and depends on the value of $D$; the trends will be the same irrespective of the model used. In this model, the second term $m_B V_m/M_B S$ is the diffusion length $L$ (geometric thickness of the electrode) for the dense electrode. For the porous composite electrode, neither diffusion length nor interface area is straightforward to estimate due to the porosity and the penetration of the electrolyte. However, the recently confirmed "sequential particle-by-particle charging/discharging" electrochemical process [14] makes total volume of the active materials over geometric electrode surface area a reasonable estimation of diffusion length.

Fig. 3a plots the chemical diffusion coefficient $D_{GITT}$ of $Li_xNi_yMn_yCo_{1-2y}O_2$ as a function of $x$ for lithium removal. The $D_{GITT}$ values decrease upon the initial stages of lithiation and reach minima when about 0.3 Li is removed. Then the $D_{GITT}$ values increase until maxima are reached. This feature of $D_{GITT}$ variation has been reported before [26–28]. The comparison shows that the lithium removal diffusivity for $Li_xNi_yMn_yCo_{1-2y}O_2$ follows the order: 333 > 442 > 992 > 550, which is consistent with the increase of Li/Ni exchange [17]. The degree of Li/Ni exchange induces the difference in lithium diffusivity, which thereby affects the rate capability for this series of compounds [17]. Fig. 3b displays the $D_{GITT}$ values of lithiation, where the composition trend is different from that of delithiation but resembles the trend of chemical diffusion coefficient for $Na_xTaS_2$ [3]. The lithiation $D_{GITT}$ for $Li_xNi_yMn_yCo_{1-2y}O_2$ are around $10^{-10}$ $cm^2\ s^{-1}$, lower than that for $Li_xCoO_2$ ($10^{-9}$ $cm^2\ s^{-1}$) and $Li_xTiS_2$ ($10^{-8}$ $cm^2\ s^{-1}$). As more lithium ions are inserted into the compound, the lithiation $D_{GITT}$ decreases due to fewer vacancies in host structure available for further lithium ions.

The PITT measurements on $LiNi_yMn_yCo_{1-2y}O_2$ in Fig. 4a and b show the voltage steps $V(t)$ and corresponding current decay $I(t)$ under each constant voltage for 442 upon charge and discharge, respectively. $LiNi_yMn_yCo_{1-2y}O_2$ compounds with other compositions show a current decay mode similar to 442. All the current relaxation curves show diffusion-limited behavior without phase-transition-limited process. This confirms the diffusion-only one-phase reaction without two-phase coexistence. Again, the different variation features were observed for charge and discharge process. From the $I(t)$ curve, the extent of current decay decreases and then increases during voltage step increments while monotonously decreasing during voltage step decrements. At certain voltage steps, the transport coefficient can be extracted from the corresponding $I(t)$ curve using well-established Cottrell's diffusion-only model for the current decay [26,35–37]:

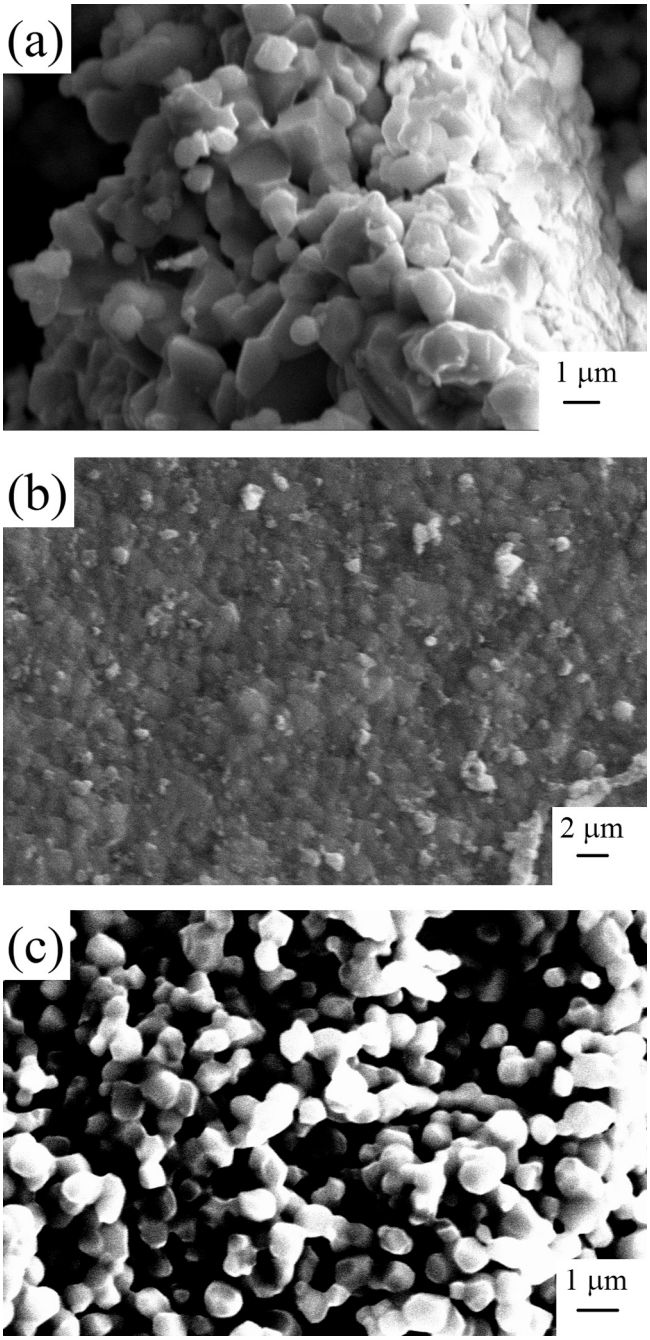


**Fig. 5.** The SEM morphology of (a) 1000 °C sintered 333 (b) 1100 °C sintered 550 and (c) 1000 °C sintered 550.

$$I(t) = \frac{\Delta Q}{\tau_D/\Lambda + \sqrt{\pi\tau_D t}}, \tau_D = L^2 \Big/ D_{PITT}, \Lambda = R_D \Big/ R_{ext} \quad (2)$$

where $\Delta Q$ is the total amount of charge transferred after a single PITT increment, $\tau_D$ is the characteristic diffusion time, $L$ is the diffusion length, $D_{PITT}$ is the chemical diffusion coefficient derived from PITT measurement, $\Lambda$ is the ratio of the diffusion resistance $R_D$ to the external resistance $R_{ext}$. The units for $I(t)$, $\Delta Q$, $\tau_D$, $R_D$, $R_{ext}$ and $t$ are mA, mA s, s, Ω and Ω, respectively. $\tau_D$ can be derived from the intercept of a linear regression on a plot of $1/(I(t)\sqrt{t})$ vs. $1/\sqrt{t}$ based on Eq. (2). The $D_{PITT}$ then can be expressed as $L^2/\tau_D$. Fig. 5c and d show the $D_{PITT}$ with respect to $L^2$ for 442 upon delithiation and lithiation. The non-cottrellian diffusion data points (no obvious linear region in $1/(I(t)\sqrt{t})$ vs. $1/\sqrt{t}$ plot) at the beginning and at the higher voltage steps in PITT were not included in this $D_{PITT}$ plots, which are possibly due to the surface reaction at the beginning and the electrolyte decomposition at voltages above 4.3 V respectively. However, the results obtained from PITT plots nicely match the results based on GITT. First of all, the variation of $D_{PITT}$ with respect to voltage between charge and discharge are very similar to that observed in the GITT experiment. The minimum region $D_{PITT}$ plots (Fig. 4c) matches the range of $0.6 \le x \le 0.8$ in $Li_xNi_{0.4}Mn_{0.4}Co_{0.2}O_2$, according to the OCV profile of 442 (Fig. 4c inset graph). Thus, the minima values of $D_{PITT}$ are also obtained in the delitation range of $0.6 \le x \le 0.8$, the same as that in the $D_{GITT}$ plots. In addition, assuming the diffusion length to be the thickness of the electrode (around 10 μm), the $D_{PITT}$ is around $10^{-10}$ $cm^2$ $s^{-1}$, which is the same magnitude as $D_{GITT}$ of 442.

### 3.3. Electronic conductivity

The preparation of samples for electronic conductivity measurements is a nontrivial process as the lithium content, structure, density and porosity are all expected to have an effect. To obtain similar pellet density for 550 and 333, we have investigated the temperature influence on the pellet density. At the same sintering temperature of 1000 °C, 550 pellet is composed of much smaller particles and larger pores than those of 333 pellet, as shown in Fig. 5a and c. However, the similar average particle size and porosity have been obtained when using 1000 °C sintered 333 pellet and the 1100 °C sintered 550 pellet, as indicated in Fig. 5a and b. The pellet densities for 1000 °C sintered 333 and 1100 °C sintered 550 are 3.89 g $cm^{-3}$ and 3.95 g $cm^{-3}$, respectively. In addition to making the pellets with similar densities, we should also have a good control of the lithium concentration in $Li_xNi_yMn_yCo_{1-2y}O_2$. The OCV of the $Li_xNi_{0.33}Mn_{0.33}Co_{0.33}O_2$ and $Li_xNi_{0.5}Mn_{0.5}O_2$ pellets in the electrochemical cells accord well with the reported OCV vs. $x$ profile [17].

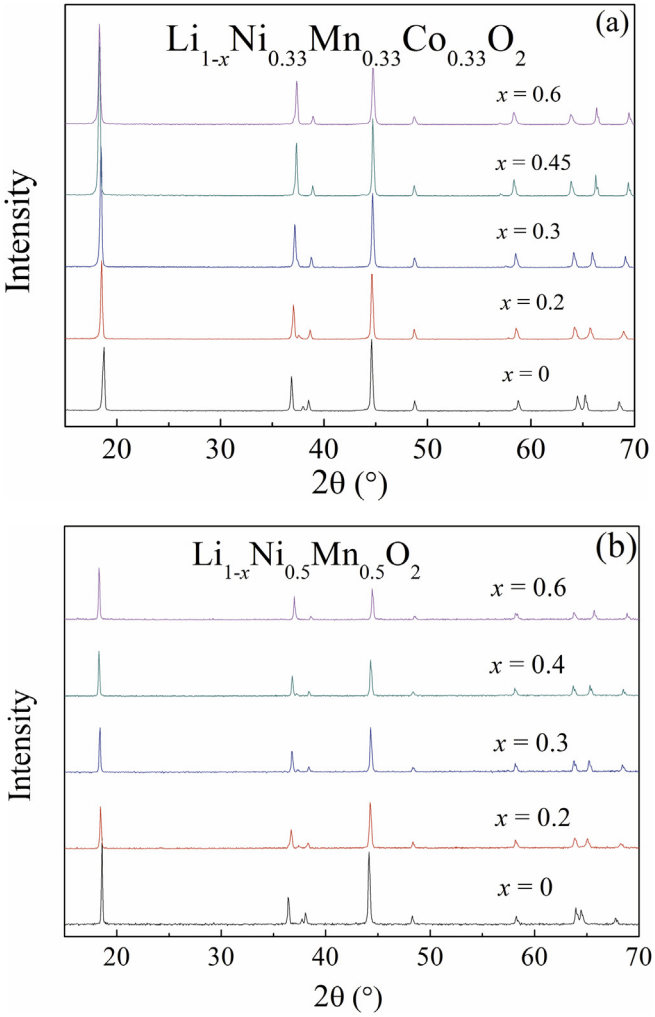


**Fig. 6.** XRD pattern of (a) $Li_{1-x}Ni_{0.33}Mn_{0.33}Co_{0.33}O_2$ ($x$ = 0, 0.2, 0.3, 0.45, 0.6) and (b) $Li_xNi_{0.5}Mn_{0.5}O_2$ ($x$ = 1, 0.2, 0.3, 0.4, 0.6).

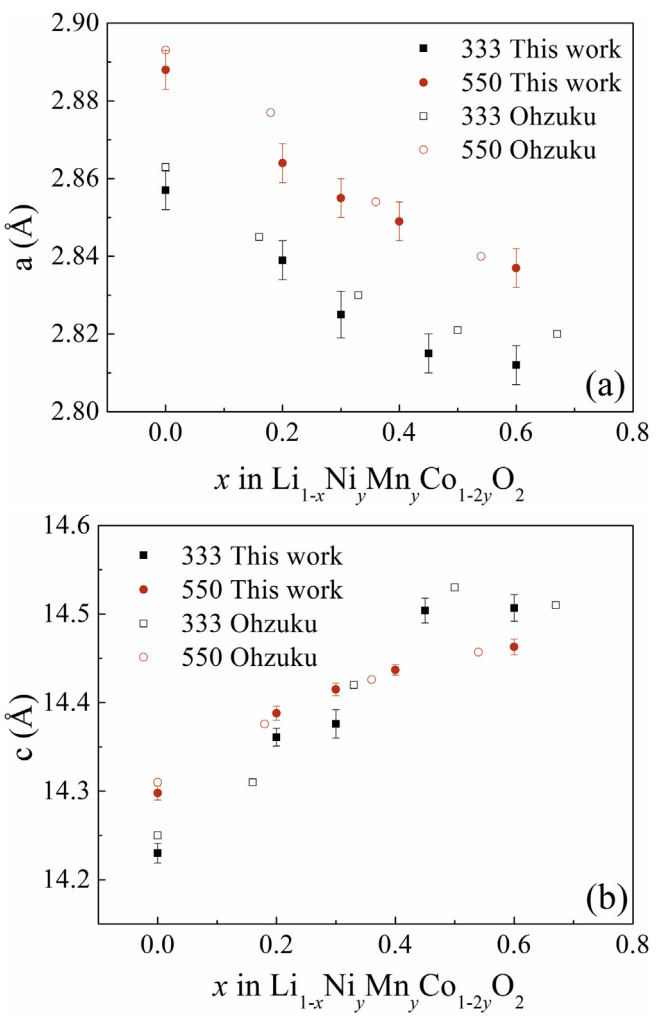


**Fig. 7.** The summarized lattice parameter (a) $a$ and (b) $c$ variation calculated from XRD pattern with the comparison of lattice parameters by Ohzuku [27,28].

The XRD patterns of the delithiated 550 and 333 pellets show no obvious impurity peaks, as displayed in Fig. 6a, b. The lattice parameter variation for the pellets, as shown in Fig. 7a and b, matches very well with the powder samples reported by Ohzuku [32,33]. It confirms that the targeted lithium concentrations in these samples have been successfully achieved.

Fig. 8a and b shows the temperature dependence of conductivity of $Li_xNi_{0.33}Mn_{0.33}Co_{0.33}O_2$ and $Li_xNi_{0.5}Mn_{0.5}O_2$. In each group of data, the conductivity increase and activation energy decrease with decreasing $x$. There is no transition to metal-like conductivity as in $Li_xCoO_2$ or cobalt-rich $Li_xNi_yCo_{1-y}O_2$ and both materials show inferior electronic conductivity compared to $Li_xCoO_2$ or cobalt-rich $Li_xNi_yCo_{1-y}O_2$ at same temperature and delithiation stage [38–40]. Comparing $Li_xNi_{0.33}Mn_{0.33}Co_{0.33}O_2$ and $Li_xNi_{0.5}Mn_{0.5}O_2$, $Li_xNi_{0.33}Mn_{0.33}Co_{0.33}O_2$ shows an order of magnitude higher conductivity than $Li_xNi_{0.5}Mn_{0.5}O_2$ for the similar $x$ value, which may largely contribute to the better rate capability for 333 compared to 550.

Within the measured temperature range, the $\log(\sigma)$ vs. $1/T$ has good linear relationship, where $\sigma$ is the conductivity, $T$ is the temperature. The activation energy of each sample was calculated by using Arrhenius equation $\sigma = \sigma_0 e^{-E_a/kT}$, where $\sigma_0$ is a constant, $E_a$ is the activation energy, and $k$ is the Boltzmann constant. This measured activation energy of $LiNi_{0.33}Mn_{0.33}Co_{0.33}O_2$ and $Li_{0.33}Ni_{0.33}Mn_{0.33}Co_{0.33}O_2$ is consistent with the calculated half band gap by Ceder's group (around 0.3 eV and 0.2 eV for $LiNi_{0.33}Mn_{0.33}Co_{0.33}O_2$ and $Li_{0.33}Ni_{0.33}Mn_{0.33}Co_{0.33}O_2$ respectively) [41]. The shrinkage of the band gap may explain the decreased activation energy of electrons, which possibly increase electronic conductivity. However, this does not exclude the small polaron conduction mechanism that is normally observed in nickel-rich $Li_xNi_yCo_{1-y}O_2$ [42], where the activation energy is not directly related to band gap but the electronic migration barrier and the binding energy between the lithium ions and the electrons. The major charge carrier and exact conduction mechanism are still unclear and oxygen involvement in the charge compensation as delithiation further complicates the conductivity interpretation [43,44].

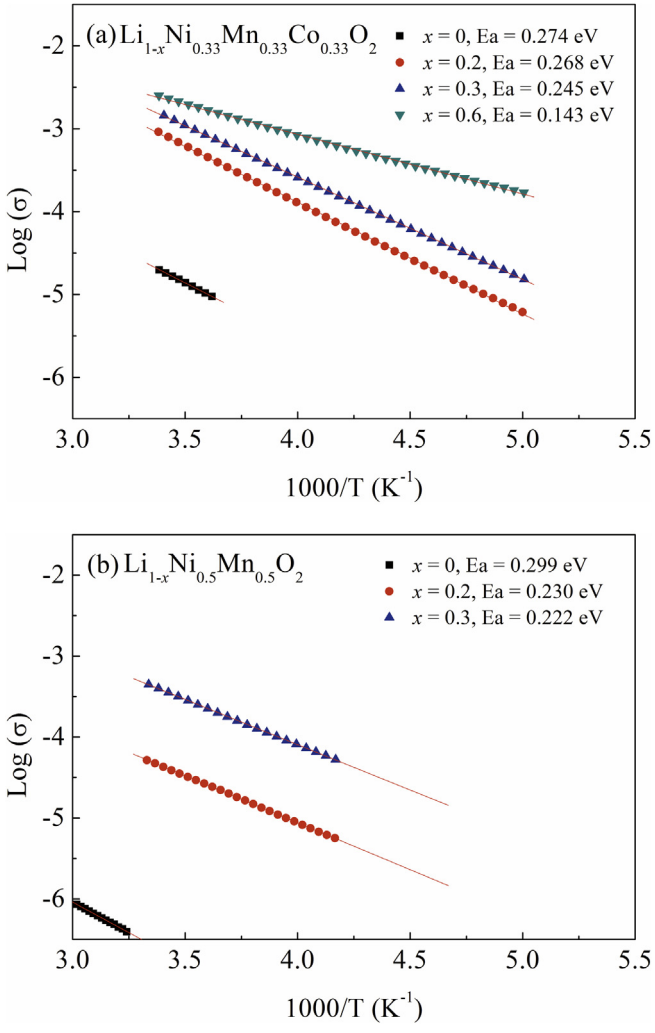


**Fig. 8.** The temperature dependence of conductivity of (a) $Li_{1-x}Ni_{0.33}Mn_{0.33}Co_{0.33}O_2$ and (b) $Li_{1-x}Ni_{0.5}Mn_{0.5}O_2$.

## 4. Conclusions

The lithium diffusivity and electronic conductivity for the series $Li_xNi_yMn_yCo_{1-2y}O_2$ compounds have been investigated, in order to better understand the relationship between intrinsic properties and rate capability. We conclude that both intrinsic factors influence the rate performance. The 333 compound has higher diffusivity and electronic conductivity and thus better rate performance than 550. Chemical diffusion coefficients for both delithiation and lithiation of $Li_xNi_yMn_yCo_{1-2y}O_2$ investigated by GITT and PITT experiments are calculated to be around $10^{-10}$ $cm^2$ $s^{-1}$, lower than that of $Li_xCoO_2$. The electronic conductivity of $Li_xNi_yMn_yCo_{1-2y}O_2$ is inferior that of $Li_xCoO_2$ at same temperature and delithiation stage. However, the $Li_xNi_yMn_yCo_{1-2y}O_2$ are able to deliver 55%–80% of theoretical capacity at 5 C with good electronic wiring in the composite electrode and make them very promising candidates for electric propulsion in terms of rate capability.

## Acknowledgment

This work at Binghamton and NREL was supported by the Assistant Secretary for Energy Efficiency and Renewable Energy, Office of Vehicle Technologies of the U.S. Department of Energy under Contract No. DE-AC02-05CH11231, Subcontract No. 6807148 and DE-AC-36-08GO28308 respectively under the Batteries for Advanced Transportation Technologies (BATT) Program.

## References

[1] M.S. Whittingham, Science 192 (1976) 1126.
[2] M.S. Whittingham, Prog. Solid State Chem. 12 (1978) 41.
[3] M.S. Whittingham, Chem. Rev. 104 (2004) 4271.
[4] A.H. Thompson, Phys. Rev. Lett. 35 (1975) 1786.
[5] Z. Yang, J. Zhang, M.C.W. Kintner-Meyer, X. Lu, D. Choi, J.P. Lemmon, J. Liu, Chem. Rev. 111 (2011) 3577.
[6] B. Dunn, H. Kamath, J.-M. Tarascon, Science 334 (2011) 928.
[7] G.L. Soloveichik, Annu. Rev. Chem. Biomol. Eng. 2 (2011) 503.
[8] Z. Li, D. Young, K. Xiang, W.C. Carter, Y.-M. Chiang, Adv. Energy Mater. 3 (2013) 290.
[9] K. Kang, Y.S. Meng, J. Bréger, C.P. Grey, G. Ceder, Science 311 (2006) 977.
[10] S.-Y. Chung, J.T. Bloking, Y.-M. Chiang, Nat. Mater. 1 (2002) 123.
[11] D. Young, A. Ransil, R. Amin, Z. Li, Y.-M. Chiang, Adv. Energy Mater. 3 (2013) 1125.
[12] C. Ban, Z. Li, Z. Wu, M.J. Kirkham, L. Chen, Y.S. Jung, E.A. Payzant, Y. Yan, M.S. Whittingham, A.C. Dillon, Adv. Energy Mater. 1 (2011) 58.
[13] C. Ban, Z. Wu, D.T. Gillaspie, L. Chen, Y. Yan, J.L. Blackburn, A.C. Dillon, Adv. Mater. 22 (2010) E145.
[14] W. Dreyer, J. Jamnik, C. Guhlke, R. Huth, J. Moškon, M. Gaberšček, Nat. Mater. 9 (2010) 448.
[15] Z. Li, N.A. Chernova, J. Feng, S. Upreti, F. Omenya, M.S. Whittingham, J. Electrochem. Soc. 159 (2011) A116.
[16] J. Xiao, N.A. Chernova, M.S. Whittingham, Chem. Mater. 20 (2008) 7454.
[17] Z. Li, N.A. Chernova, M. Roppolo, S. Upreti, C. Petersburg, F.M. Alamgir, M.S. Whittingham, J. Electrochem. Soc. 158 (2011) A516.
[18] J. Xiao, N.A. Chernova, M.S. Whittingham, Chem. Mater. 22 (2010) 1180.
[19] K.C. Kam, A. Mehta, J.T. Heron, M.M. Doeff, J. Electrochem. Soc. 159 (2012) A1383.
[20] T.E. Conry, A. Mehta, J. Cabana, M.M. Doeff, Chem. Mater. 24 (2012) 3307.

[21] H. Yu, Y. Qian, M. Otani, D. Tang, S. Guo, Y. Zhu, H. Zhou, Energy Environ. Sci. 7 (2014) 1068.
[22] W. Weppner, R.A. Huggins, J. Electrochem. Soc. 124 (1977) 1569.
[23] K.M. Shaju, G.V.S. Rao, B.V.R. Chowdari, J. Electrochem. Soc. 151 (2004) A1324.
[24] K.M. Shaju, G.V. Subba Rao, B.V.R. Chowdari, Electrochim. Acta 49 (2004) 1565.
[25] N. Yabuuchi, S. Kumar, H.H. Li, Y.-T. Kim, Y. Shao-Horn, J. Electrochem. Soc. 154 (2007) A566.
[26] N. Meethong, Y.-H. Kao, W.C. Carter, Y.-M. Chiang, Chem. Mater. 22 (2010) 1088.
[27] Y.-I. Jang, B.J. Neudecker, N.J. Dudney, Electrochem. Solid-State Lett. 4 (2001) A74.
[28] H. Xia, L. Lu, G. Ceder, J. Power Sources 159 (2006) 1422.
[29] B.H. Toby, J. Appl. Crystallogr. 34 (2001) 210.
[30] A.C. Larson, R.B.V. Dreele, in: Los Alamos Natl. Lab. Rep. LAUR, 1994, pp. 86–748.
[31] D.D. MacNeil, Z. Lu, J.R. Dahn, J. Electrochem. Soc. 149 (2002) A1332.
[32] K. Ariyoshi, T. Ichikawa, T. Ohzuku, J. Phys. Chem. Solids 69 (2008) 1238.
[33] T. Ohzuku, A. Ueda, N. Yamamoto, J. Electrochem. Soc. 142 (1995) 1431.
[34] S.-C. Yin, Y.-H. Rho, I. Swainson, L.F. Nazar, Chem. Mater. 18 (2006) 1901.
[35] M.D. Levi, R. Demadrille, A. Pron, M.A. Vorotyntsev, Y. Gofer, D. Aurbach, J. Electrochem. Soc. 152 (2005) E61.
[36] M.A. Vorotyntsev, M.D. Levi, D. Aurbach, J. Electroanal. Chem. 572 (2004) 299.
[37] C. Montella, J. Electroanal. Chem. 518 (2002) 61.
[38] M. Ménétrier, I. Saadoune, S. Levasseur, C. Delmas, J. Mater. Chem. 9 (1999) 1135.
[39] I. Saadoune, C. Delmas, J. Mater. Chem. 6 (1996) 193.
[40] I. Saadoune, C. Delmas, J. Solid State Chem. 136 (1998) 8.
[41] B.J. Hwang, Y.W. Tsai, D. Carlier, G. Ceder, Chem. Mater. 15 (2003) 3676.
[42] I. Saadoune, M. Ménétrier, C. Delmas, J. Mater. Chem. 7 (1997) 2505.
[43] W.-S. Yoon, M. Balasubramanian, K.Y. Chung, X.-Q. Yang, J. McBreen, C.P. Grey, D.A. Fischer, J. Am. Chem. Soc. 127 (2005) 17479.
[44] C.F. Petersburg, Z. Li, N.A. Chernova, M.S. Whittingham, F.M. Alamgir, J. Mater. Chem. 22 (2012) 19993.